International Journal of Nanoelectronics and Materials
Volume 14, No. 2, April 2021 [149-158]

Effect of KOH Molarity on Structure, Morphology, and Optical Properties of Flower-Like CuO Nanostructures Synthesized by Ultrasonic-Assisted Precipitation Method

Akhiruddin Maddu*, Ahmad Habibi, Irmansyah

Department of Physics, Faculty of Mathematics and Natural Sciences, Bogor Agricultural University, Dramaga, Bogor 16680, Indonesia

Received 18 August 2020, Revised 20 October 2020, Accepted 5 November 2020

ABSTRACT

This paper reports the effect of KOH molarity variation on structure, morphology, and optical properties of CuO nanostructures synthesized by ultrasonic-assisted precipitation method. The results of the XRD analysis showed that the CuO samples had a monoclinic structure with lattice constants which decreased with increasing KOH molarity in the sonochemical precursors. The average crystallite size (ACS) of the CuO samples depend on the KOH molarity, which tends to decrease (in the range 16-23 nm) with increasing KOH molarity. Small ACS indicates that the CuO samples tend to have a nanocrystal structure. The morphology of the CuO samples is also influenced by the KOH molarity, which the flower-shaped CuO nanostructure was found for low molarity (0.25 M) of KOH in the sonochemical precursor. The optical characteristics of CuO samples strongly absorb the wide spectrum of electromagnetic waves below 650 nm. The bandgap energy of the CuO samples has a fairly large value and fluctuates in the range of 1.74 - 1.82 eV which varies with the molarity of KOH in the precursor solutions.

Keywords: *CuO nanostructure, flower-like morphology, KOH, sonochemistry*

1. INTRODUCTION

CuO is one of the earliest semiconductor material that has been studied and applied intensively in many technology applications. CuO is well known as a p-type metal oxide semiconductor that has unique electronic and optical properties with bandgap energy in a wide range of 1.2 - 2.0 eV [1-3]. CuO has a monoclinic crystal with a lattice constant a = 4.68 Å, b = 3.42 Å, c = 5.13 Å and a density of 6,315 g/cm^3 [4-7]. Electrical conductivity, optical absorption, and photoluminescence properties of CuO semiconductors have been well known [8,9]. For a long time, CuO has been utilized in many applications including in gas sensor devices [1,10], humidity sensors [11], solar cells devices [2], photocatalysts for dye removal [12], lithium battery electrodes [13], supercapacitor electrodes [14], and antimicrobial agent [15].

Currently, CuO has been developed intensively in the form of nanostructured materials for wider applications. The various forms of CuO nanostructures currently being developed include thin

* Corresponding Author: akhiruddin@apps.ipb.ac.id

films [3,7,8,16], nanowires [11,17], nanorods [1,18], nanotubes [19], nanocubes [4], nanoflowers [13-15], nanocrystals [20], and nanoparticles [4,9,11,21-30].

The nanostructured CuO synthesis has been carried out by various methods such as sol-gel [21,22], hydrothermal [23], SILAR [8], sonochemistry [11,24,25], simple precipitation [26], electrochemical methods [27], green synthesis [28,29], microwave irradiation [30], and sputtering [31]. Each of these methods produces CuO nanostructures with unique characteristics and their respective advantages.

In this study, flower-like CuO nanostructures were synthesized by a simple precipitation method assisted by ultrasonic wave irradiation in the presence of KOH in precursor solutions. The aim of this study was to investigate the effect of the molarity of KOH content in the sonochemical precursor solution on the formation and characteristics of flower-like CuO nanostructures.

2. METHODS

2.1. Synthesis of CuO nanostructures

The synthesis of CuO nanostructures was carried out by ultrasonic-assisted precipitation method in the ultrasonic bath. 100 ml of CuNO3 (0.4 M) was prepared in a beaker glass and polyethylene glycol (PEG) (0.002 M) was added. PEG is a surfactant to disperse CuO particles. Into the mixed solution, KOH was added with four variations of molarity - 0.25 M, 0.50 M, 0.75 M, and 1 M respectively. The mixed solution was stirred using a magnetic stirrer with a rotation speed of 300 rpm for 5 minutes. A beaker glass containing a precursor solution was placed in an ultrasonic bath filled with sufficient water for sonochemical treatment at 25 kHz. The sonochemical process was maintained for 2 hours in the ultrasonic bath. Starting from room temperature, the temperature of the precursor solution in the ultrasonic bath increased during the sonication process to 75 °C. The suspension was cooled to room temperature, then washed with distilled water and filtered using filter paper. The filtrate was dried on the hot plate at 90 °C for 1 hour to obtain a gray-black CuO powder. The CuO powder was heated in a furnace at 200 °C for 2 hours. All samples with different molarity of KOH content in the precursor solution underwent the same heating treatment.

2.2. Crystal and morphology characterizations

CuO powder samples that had been successfully synthesized by ultrasonic-assisted precipitation method were characterized to investigate their crystal structure and morphology. Investigation of crystal structure was conducted by X-ray diffraction (XRD) to determine the crystal phase, the lattice parameters and average crystal size (ACS) of each CuO samples. The lattice constants, as one of the crystal parameters, were calculated by using the Cohen method, while the average crystal size (ACS), as another crystal parameter, was calculated by using Scherrer's method based on the broadening of the X-ray diffraction pattern of the CuO samples. The determination of ACS of CuO samples can be done using the Scherrer's equation (1):

$$ACS = (0.94\,\lambda)/(\beta \cos\theta) \quad (1)$$

where β is the FWHM (Full-Width at Half Maximum), λ is the wavelength of X-ray from a Cu source (1.5406 Å), and θ is the diffraction angle.

To observe their morphology, the CuO samples were scanned by scanning electron microscopy (SEM) with a 20,000 magnification using Carl Zeiss AG - EVO®50 HV-SEM at 30 kV. The images ware taken in secondary electron mode from which the surface morphology can be observed including the shape, size, and distribution of the granules.

2.2. Optical characterization

To explore their optical properties, the CuO nanostructure samples were formed into films on a slide glass substrate using spin-coating techniques from CuO colloidal suspensions. Then, the absorption spectra were measured using a Vis-NIR spectrophotometer (Ocean Optics USB2000). The absorbance spectra obtained were used to determine the bandgap energy of nanostructured CuO samples using the Tauc formula:

$$(\alpha h\nu)^{1/n} = A(h\nu - E_g) \quad (2)$$

where E_g is the bandgap energy (eV) of the CuO films, h is the Planck constant (4.135×10^{-15} eV.s), A is a constant, ν is the photon frequency (Hz), α is the absorption coefficient and n is a number representing either direct or indirect electronic transitions. For direct transitions, n=1/2, while for indirect transitions, n=2. CuO is known as a direct bandgap semiconductor [20,31], so n=1/2 is used to calculate the bandgap energy (E_g). The E_g value is determined by the extrapolation the linear portion of the Tauc plot curve to the axis of the photon energy (hv).

The thickness of CuO films was determined using the gravimetric method. Initially, the glass substrate that has not been coated with CuO is weighed and marked as mass M1, then the glass substrate that has been coated with CuO is weighed and marked as mass M2. Then, the CuO film thickness is determined using the following relation:

$$d = (M1-M2)/(\rho.A) \quad (3)$$

where ρ is the density of the CuO films (6,315 g/cm^3) [7], and A is the area of the films deposited on the surface of the glass substrates.

3. RESULTS AND DISCUSSION

3.1 Crystal structure and morphology

The effect of KOH molarity in sonochemical precursors on the crystal properties of the CuO samples was investigated based on the X-ray diffraction analysis. Figure 1 shows the XRD pattern of the CuO samples for each variation of KOH molarity in the precursors (0.25; 0.5; 0.75; 1 M). In general, there were almost no differences in the diffraction patterns of all samples. All peaks in the diffraction pattern can be easily identified as the peak of the CuO crystal phase with a fairly sharp spectrum, although there is a slight spectrum broadening. The diffraction pattern well matches to the CuO monoclinic structure (JCPDS Card No. 65-2309) [2,4,13,20,31-33]. The diffraction spectra scanned in angle 2θ from 30^o to 70^o show diffraction peaks corresponding to the lattice planes (110), (-111), (111), (-202), (020), (202), (-113), (-311), and (220), respectively. The two highest peaks of the lattice planes (-111) and (111) confirmed that the monoclinic CuO crystals have grown well. There is no Cu_2O phase in the diffraction pattern so it can be concluded that the resulting samples are pure CuO phase with a monoclinic structure.

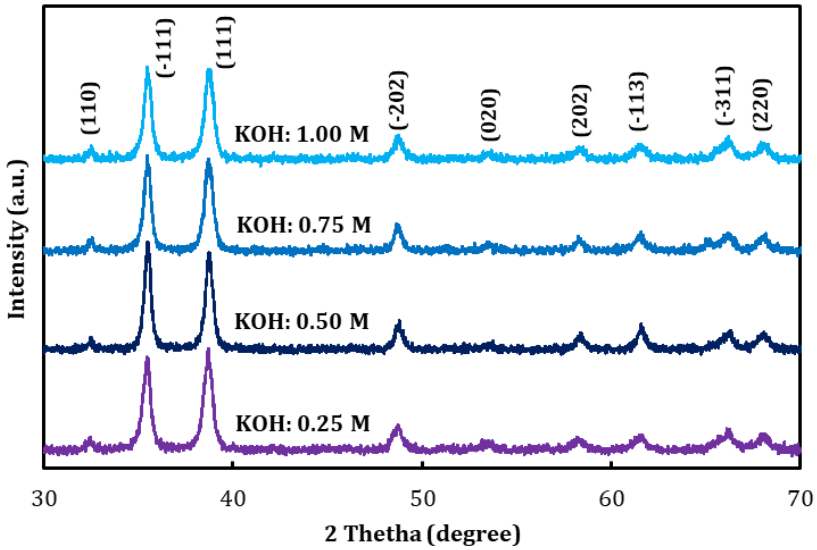

Figure 1. X-ray diffractogram of CuO samples with different KOH concentration (0.25 M, 0.5 M, 0.75 M and 1.0 M).

The effect of KOH molarity in sonochemical precursor solutions on the crystal properties of CuO was also investigated to lattice constants. The lattice constants of the CuO samples were determined based on the Miller index obtained from the X-ray diffraction pattern using the Cohen method. The calculating results of the lattice constants of the CuO sample are summarized in Table 1. The constant a is in the range 4.50 Å - 4.52 Å, constant b in the range of 3.50 Å - 3.52 Å, and constant c in the range of 5.46 Å - 5.5 Å. These calculation results were slightly different with the lattice constants in the reference data on the JCPDS Card No. 45-0937, where the lattice constants a = 4.68 Å, b = 3.42 Å and c = 5.13 Å [4,7].

The lattice constant a for all samples is smaller than the database, while the lattice constants b and c are greater than the database [15,17]. This means that all samples underwent growth inhibition in the direction of the x-axis. In general, the lattice constants tend to decrease with KOH molarity, even though there are fluctuations in the lattice constants with KOH molarity. The decrease in the lattice constant is caused by the inhibition of the crystal growth due to the presence of KOH in the precursor solution.

Table 1. The lattice parameters and ACS values of the CuO samples for the peak of (-111) plane

Conc. of KOH (M)	Lattice parameters (Å)			ACS (nm)
	a	**b**	**c**	
0.25	4.52	3.52	5.51	17.24
0.5	4.50	3.51	5.50	23.25
0.75	4.52	3.50	5.51	19.59
1.0	4.50	3.50	5.46	16.95

The calculation results of the ACS values for the peak of (-111) plane at 2θ=35.76 using the Scherrer equation (1) indicated that the presence of KOH in sonochemical precursors affected the ACS values of CuO samples, as are summarized in Table 1. The crystal size of all CuO samples obtained is relatively small (below 25 nm) corresponding to the broadening of the diffraction patterns, therefore it can be considered that the grown CuO has nanostructures.

The data tendency shows that the ACS of CuO fluctuates with KOH molarity in the sonochemical precursor solution. Initially, the ACS increased when the KOH molarity increased from 0.25 M to

0.5 M (the largest ACS), then decreased when the KOH molarity increased to 0.75 M to 1 M. The addition of KOH at 0.5 M molarity is considered as an optimal condition for increasing the ACS. Further addition of KOH with the highest molarity (0.75 M and 1 M) significantly reduced the ACS of CuO, due to the crystal growth inhibited when the amount of KOH in the precursor solution was too large (saturation condition).

The surface morphology of the CuO samples was taken with a scanning electron microscope (SEM) with a magnification of 20,000 times. Figure 2 shows the SEM images of four CuO samples with different KOH molarities in precursor solutions. The sample with the lowest KOH molarity (0.25 M) shows a very different morphology compared to the other three samples. The morphology of the CuO sample with the lowest KOH molarity (0.25 M) shows a flower-shaped structure (Figure 2a), while other samples show the flakes morphology. It can be concluded that the formation of a flower-shaped structure can occur at low KOH molarity. Higher KOH molarity in sonochemical precursors produces abundant alkali concentrations, hence faster process, so the formation of flower-shaped CuO nanostructures cannot be controlled.

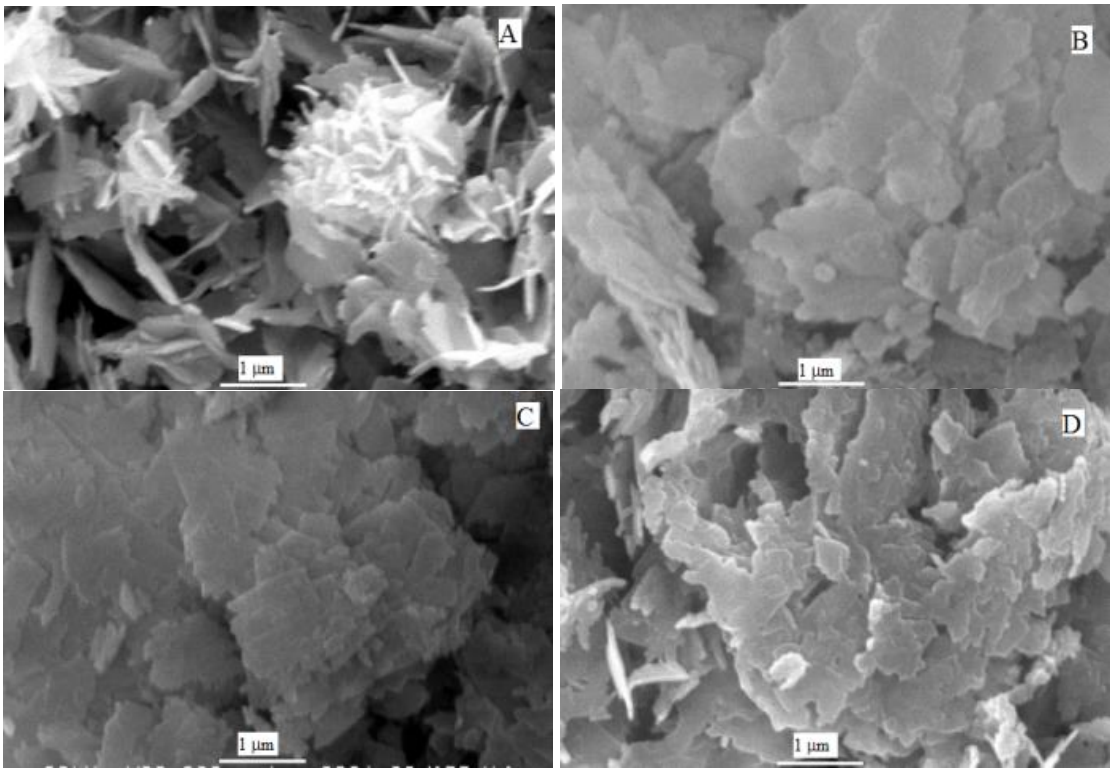

Figure 2. SEM Photographs of CuO samples with different concentrations of KOH: (A) 0.25 M, (B) 0.5 M, (C) 0.75 M, and (D) 1.0 M

3.2 Optical properties

The optical properties of CuO samples were explored by measuring the absorbance characteristics of CuO films using a Vis-NIR spectrophotometer (USB2000 Ocean Optics). Figure 3 shows the absorption spectra of CuO films with variations in the molarity of KOH in sonochemical precursors. Based on the absorption characteristics obtained, it was found that all samples absorbed the electromagnetic spectrum in a fairly long range below 650 nm, similar to some previous studies [8,21-32]. The edge of the absorption band is around 650 nm which shows that the bandgap of CuO films is in a wide range of values.

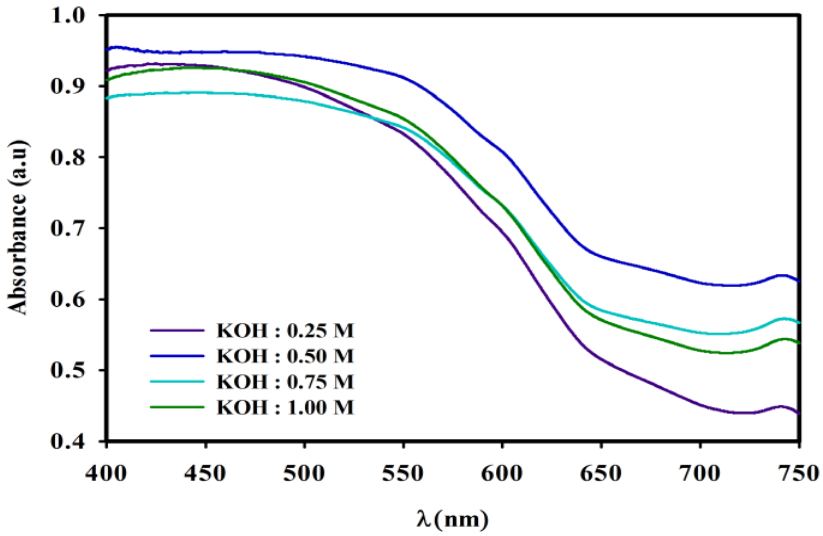

Figure 3. Absorption spectra of CuO films with different concentration of KOH: 0.25 M, 0.5 M, 0.75 M and 1.0 M

Bandgap energy (Eg) of CuO films was determined by using the relationship between absorption coefficient (α) and photon energy (hv). The absorption coefficient (α) is calculated using the relationship $\alpha = 2.3026 (A/x)$, where A is the absorbance of the film at each wavelength, and x is the thickness of the film. Bandgap energy is determined by a plot between $(\alpha hv)^2$ and photon energy (hv), known as the Tauc plot. Figure 4 shows a curve $(\alpha hv)^2$ versus photon energy (hv) for each CuO film with different KOH molarity in the precursor solutions. The intersection of the linear part of the curve with the photon energy axis (hv) is the bandgap energy of the CuO film.

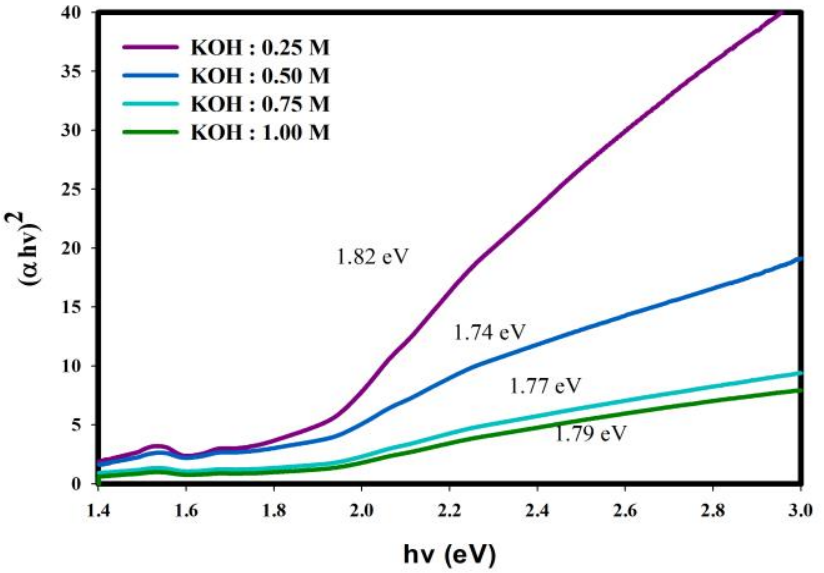

Figure 4. Tauc plot of $(\alpha hv)^2$ versus photon energy (hv) for CuO films with different concentration of KOH: 0.25 M, 0.5 M, 0.75 M and 1.0 M

Table 2. Optical band gap of the CuO samples.

Conc. of KOH (M)	Bandgap energy (eV)
0.25	1.82

0.5	1.74
0.75	1.77
1.0	1.79

In general, the bandgap energy of synthesized CuO samples is relatively larger than most others literature (around 1.2 eV) [1,2]. However, some literature also reports relatively large bandgap energy of CuO,[1-3] similar to that found in this work. The Tauc plot shows that the bandgap energy of the CuO sample is in the range of 1.74 - 1.82 eV which varies depending on the KOH molarity in sonochemical precursor solutions, as presented in Table 2. These bandgap energies fluctuate with the KOH molarity in the precursor solution, initially, the bandgap energy of CuO was 1.82 eV at 0.25 M KOH molarity, then decreased with increasing KOH (0.5M) molarity to 1.74 eV. This decrease is estimated due to the crystallite size of the CuO is enlarged. Then, the bandgap energy increases when the KOH molarity increases further (0.75 and 1 M), although it does not reach the lowest value such as when the KOH molarity is 0.25 M.

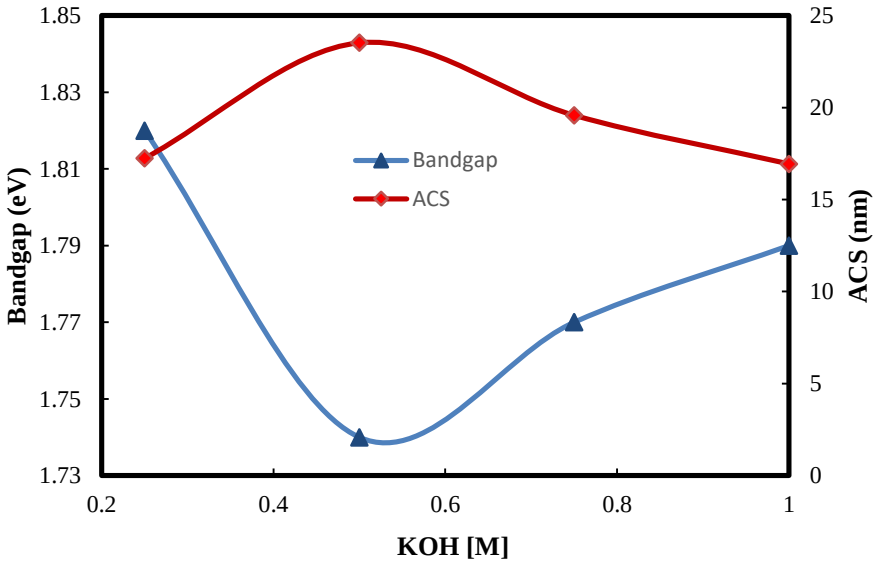

Figure 5. Curves between KOH molarities versus bandgap energy (E_g) and average crystallite size (ACS) of CuO nanocrystals

Figure 5 shows a combined curve between bandgap energy and the crystal size of CuO with KOH molarity in the precursor solutions. Bandgap energy correlates with the crystal size of the CuO, when the crystal size is small the bandgap energy is large and vice versa, this corresponds to what is predicted by the quantum confinement effect [35]. On the other hand, the relationship between bandgap energy versus KOH molarity is in-verse with the relationship between ACS versus KOH molarity in sonochemical precursor solutions. This result confirms that the addition of KOH into sonochemical precursor solutions affects the crystal size which in turn affects the bandgap energy of CuO. As discussed earlier, the ACS of CuO varies with the molarity of KOH in the precursor solution. In this study, there is an inverse relationship between the ACS and bandgap energy of CuO on the variation of KOH molarity, where when the ACS is small the bandgap energy is large, and vice versa.

CONCLUSION

Flower-like CuO nanostructures has been successfully synthesized by the ultrasonic-assisted precipitation method. The presence of KOH in sonochemical precursors affected the structure, morphology and optical properties of CuO. Lattice constants tend to decrease with increasing KOH molarity in the sonochemical precursor solution. Meanwhile, the average

crystallite size (ACS) of CuO also varies with the molarity of KOH in the precursor solution, where the greatest ACS was obtained when the KOH molarity was 0.5 M in the precursor solution. On the other hand, the flower-like morphology was obtained when the molarity of KOH is 0.25 M in the precursor solution. Thus, the formation of flower-like CuO morphology is obtained when the molarity of KOH is low. The optical properties of CuO are also influenced by the molarity of KOH in precursor solutions. Bandgap energy is quite large and also varies with KOH molarity in sonochemical precursor solutions. Bandgap energy correlates with the crystal size of CuO, where when the crystal size is small, the bandgap energy is large, and vice versa.

REFERENCES

[1] Park S., Ko H., An S., Lee W.I., Lee, S., Lee, C., Ceram. Int., 39 (2013) 5255-5262.
[2] Ganga, B.G., Santhosh, P.N., Mater Lett., 138 (2015) 113-115.
[3] Bhaumik, A., Haque, A., Karnati, P., Taufique, M.F.N., Patel, R., Ghosh K., Thin Solid Films 572 (2015) 126-133.
[4] Dhineshbabu, N.R., Rajendran, V., Nithyavathy, N., Vetumperumal, R., Appl. Nanosci., 6 (2016) 933-939.
[5] Akgul, F.A., Akgul, G., Yildirim, N., Unalan, H.E., Turan, R., Mater. Chem. Phys., 147(3) (2014) 987-995.
[6] Zhang, Q., Zhang, K., Xu, D., Yang, G., Huang, H., Nie, F., Liu, C., Yang S., Prog. Mater. Sci., 60 (2014) 208-237.
[7] Tombak, A., Benhaliliba, M., Ocak, Y.S., Kiliçoglu, T., Results in Physics 5 (2015) 314-321.
[8] Visalakshi, S., Kannan, R., Valanarasu, S., Kathalingam, A., Mater. Res. Innov., 21(3) (2017) 146-151.
[9] Son, D.I., You, C.H., Kim, T.W., App. Surf. Sci., 255 (2099) 8794-8797.
[10] Rydosz, A., Coatings 8 (2018) 425.
[11] Gu, Y., Jiang, H., Ye, Z., Sun, N., Kuang, X., Liu, W., Li, G., Song, X., Zhang, L., Bai, W., Tang, X., Electron. Mater. Lett., 16 (2020) 61–71.
[12] Farbod, M., Ghaffari, N.M., Kazeminezhad I., Mater. Lett., 81 (2012) 258-260.
[13] Wang, L., Tang, K., Zhang, M., Zhang, X., Xu, J., Func. Mater. Lett., 7(6) (2014) 1440008 (3 pages).
[14] Dubal, D.P., Gund, G.S., Lokhande, C.D., Holze, R., Mater. Res. Bull., 48 (2013) 923-928.
[15] Mageshwari, K., Sathyamoorthy, R., J. Mater. Sci. Tech., 29 (2013) 909-914.
[16] Bayansal, F., Cetinkara, H.A., Kahraman, S., Cakmak, H.M., Guder, H.S., Ceram. Int., 38 (2012) 1859-1866.
[17] Ethiraj, A. S., Kang, D.J., Nano Res. Lett., 7 (2012) 70.
[18] Chen, H., Zhao, G., Liu, Y., Mater. Lett., 93 (2013) 60-63.
[19] Park, S., Kim, S., Park, S., Lee, C., Mater. Lett., 138 (2015) 110-112.
[20] Hassan, M.S., Amna, T., Yang, O-B., El-Newehy, M.H., Al-Deyabd, S.S., Khil, M.S., Coll. Surf. B: Biointerfaces 97 (2012) 201-206.
[21] Kayani, Z.N., Umer, M., Riaz, S., Naseem, S., J. Electron. Mater., 44 (2015) 3704-3709.
[22] Etefagh, R., Azhir, E., Shahtahmasebi, N., Scientia Iranica F 20(3) (2013) 1055–1058.
[23] Outokesh, M., Hosseinpour, M., Ahmadi, S.J., Mousavand, T., Sadjadi, S., Soltanian, W., Ind. Eng. Chem. Res., 50 (2011) 3540-3554.
[24] Ranjbar-Karimi, R., Bazmandegan-Shamili, A., Aslani, A., Kaviani, K., Physica B: Condensed Matter., 405 (2010) 3096-3100.
[25] Zou, Y., Li, Y., Guo, Y., Zhou, Q., An, D., Mater. Res. Bull., 47 (2012) 3135-3140.
[26] Rahnam, A., Gharagozlou, M., Opt. Quant. Electron., 44 (2012) 313-322.
[27] Katwal, R., Kaur, H., Sharma, G., Naushad, M., Pathania, D., J. Ind. Eng. Chem., 31 (2015) 173-184.
[28] Tavakoli, S., Kharaziha, M., Ahmadi, S., J. Nanostruct., 9(1) (2019) 163-171.
[29] Raja Naika, H., Lingaraju, K., Manjunath, K., Kumar, D., Nagaraju, G., Suresh, D., Nagabhushana, H., J. Taibah Univ. Sci., 9 (2015) 7–12.

[30] Sutradhar, P., Saha, M., Maiti, D., J. Nanostruct. Chem., 4 (2014) 86.
[31] Cho, S., Met. Mater. Int., 19 (2013) 327-1331.
[32] Zhu, G., Xu, H., Xiao, Y., Liu, Y., Yuan, A., Shen, X., ACS Appl. Mater. Interfaces., 4 (2012) 744−751
[33] Wang, F., Li, H., Yuan, Z., Sun, Y., Chang, F., Deng, H., Xie, L., Li, H., RSC Adv.**,** 6 (2016) 79343-79349
[34] Fang, J., Xuan, Y., RSC Adv., 7 (2017) 56023-56033.
[35] Ahmed, A.M., Rabia, M., Shaban, M., RSC Adv., 10 (2020) 14458-14470